Complex Image Model for Ground-Penetrating Radar Antennas

Christopher J. Leat, Nicholas V. Shuley, and Glen F. Stickley

***Abstract*—A method of combining the complex image method with the constant Q assumption is derived, which enables the calculation of complex image parameters once for the whole frequency range in the general half-space case. The mixed potential method of moments is then used to model horizontal wire dipoles near a lossy half-space, using pulse-basis functions and point matching. The method is demonstrated by the modeling of two types of wire dipole. A conductive half-wave dipole shows excellent agreement with NEC-3. The current distribution of a 3.4 m resistively loaded dipole across the frequency range 0–512 MHz is also calculated and transformed to the time domain. The result agrees with published measurements. The time required on a work station was reduced to 4/ s per frequency point.**

***Index Terms*—Moment methods, radar antennas.**

I. Introduction

THIS work draws upon two observations. First, for many rock and soil materials, the complex permittivity is approximately constant over the range of frequencies used in ground penetrating radar (GPR). Second, the half-space model, which assumes that the ground is homogeneous, is a useful model for GPR antennas that captures to first order the interaction of the antenna with the ground surface.

The observation that conduction and displacement currents bear an approximately constant ratio to each other over GPR frequency bands has been used for attenuation calculations of GPR pulses [1] where it has become known as the *constant Q assumption*. Consideration of the same data, however, also suggests the use of the stronger assumption that *complex permittivity may be considered constant to good approximation* in the modeling of antennas and scatterers.

In support of the second observation, we note that although the ground is, in general, not homogeneous, the half-space model has been frequently used in the GPR context. Scatterer [2], [3] and antenna [4] studies have both adopted the simplification of a homogeneous ground material. In addition, the half-space model has a long ancestry in the analysis of broadcast antennas, which operate at low frequencies and, thus, are necessarily close to the ground.

Some applications outside GPR also involve the combination of the half-space and constant complex permittivity. Planar antennas on thick substrates [5] are a recent example. The combination enables the efficient reuse of Green's functions across the frequency range and the reuse is particularly convenient in the case of the complex image method [6].

As an application of the method, a practical GPR antenna is modeled with the emphasis on minimal computational requirements. A resistive dipole of up to six wavelengths in length, in close proximity to the half-space, is shown to agree with published results although it is not obvious that complex images should function adequately alone at this range.

The method of complex images was also adopted by Vitebskiy *et al.* to model the similar problem of scattering from wires [2] and bodies-of-revolution [3], however, we suggest the use of a constant complex permittivity assumption to further improve the speed of calculation of the half-space Green's functions at each frequency, and demonstrate the application of the method to the GPR antenna.

The numerical analysis of wire antennas near a dielectric half-space has been approached in various ways. Michalski [7] used a numerically integrated MPIE formulation to model an oblique half-wave dipole antenna as a function of angle. Lindell [8] used a continuous image source intensity for the Green's function and the induced electromotive force (EMF) method to calculate the impedance of horizontal dipoles. Bourke *et al.*, [9] precalculated the Sommerfeld integrals at a grid of ρ and z values and used interpolation to speed the application of the method of moments to the modeling of currents on thin wires; this approach was incorporated into NEC which Turner [10] used to model half-wave dipole input resistance as a function of height above a lossy half-space. Popovic *et al.*, [11] used entire domain polynomial basis functions and an unspecified "compact algorithm" to evaluate the Sommerfeld integrals.

II. Mixed-Potential Green's Functions

Both scalar and vector potential Green's functions, in the half-space containing the source, may be represented as the sum of a free-space wave and the Hankel transform of an appropriate spectral reflection coefficient. Consider Fig. 1. Using cylindrical coordinates and following the notation used in Chew [12] the Green's functions can be written independently

Manuscript received August 26, 1996; revised April 13, 1998. This work was supported in part by the Step Frequency Ground Penetrating Radar Project, under the Generic Technology Grant Agreement 16040 between the Industry Research and Development Board, The University of Queensland, Mitec Australia Ltd., Technology Resources Pt. Ltd. (CRA Ltd.), Georadar Research Pt. Ltd., and the Cooperative Research Centre for Sensor Signal and Information Processing (CSSIP).

C. J. Leat and G. F. Stickley are with the Department of Electrical and Computer Engineering, The University of Queensland, Queensland, Australia 4072 and the Cooperative Research Center for Sensor Signal and Information Processing.

N. V. Shuley is with the Department of Electrical and Computer Engineering, The University of Queensland, Queensland, Australia 4072.

Publisher Item Identifier S 0018-926X(98)07496-1.

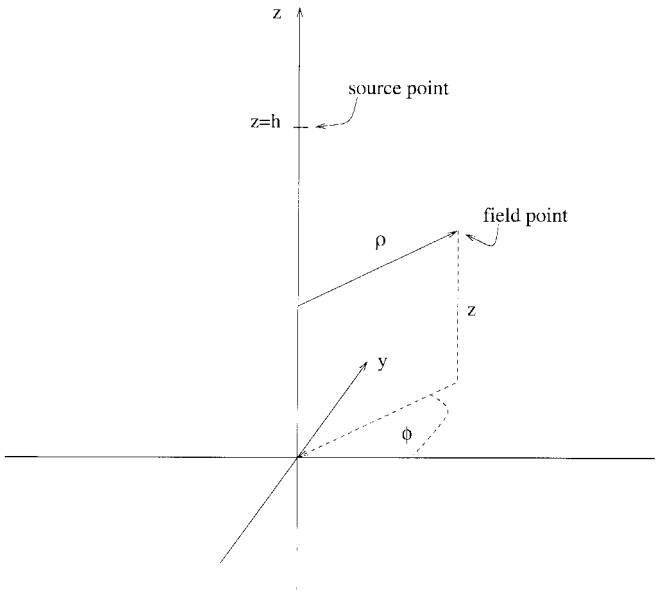

Fig. 1. Cylindrical geometry used to describe source and field points.

of ϕ

$$G = G((\rho, z), (0, h)) = \alpha\left\{\frac{e^{ikR}}{R} + i\int_0^\infty dk_\rho \frac{k_\rho}{k_{1z}} \cdot J_0(k_\rho\rho)\,\exp(ik_{1z}(z+h))R_{12}\right\} \quad (1)$$

where

$$k_\rho^2 + k_{1z}^2 = k_1^2$$

$$R^2 = \rho^2 + (z-h)^2$$

The term R_{12} is a plane wave reflection coefficient defined below and the reflecting surface lies in the $z = 0$ plane. The harmonic time dependency e^{-iwt} is assumed.

For a horizontal wire antenna, as is the case in many GPR systems, only two potentials are required. By comparing Michalski [7, eq. (1)] with [7, eqs. (49) and (51)] it is apparent that in the case of the scalar potential, G_q

$$\alpha = \frac{1}{4\pi\epsilon} \quad (2)$$

$$R_{12} = \frac{2k_{1z}}{\epsilon_r k_{1z} + k_{2z}} - 1 \quad (3)$$

and for the vector potential, G_{xx}^A

$$\alpha = \frac{\mu}{4\pi} \quad (4)$$

$$R_{12} = \frac{k_{1z} - k_{2z}}{k_{1z} + k_{2z}} \quad (5)$$

where in the above

$$k_\rho^2 + k_{2z}^2 = k_2^2. \quad (6)$$

A. Complex Image Approximations

Chow *et al.*, [6] have provided an approximate analytical method of integrating (1) that is accurate for the near and intermediate field. Before applying the method to the scalar potential reflection coefficient, it is necessary to remove the quasistatic image

$$G_{qs} = \frac{1}{4\pi\epsilon}\frac{1-\epsilon_r}{1+\epsilon_r}\frac{e^{ikR_{qs}}}{R_{qs}} \quad (7)$$

where

$$R_{qs}^2 = \rho^2 + (z+h)^2. \quad (8)$$

As outlined in Chow *et al.* [6], the complex image method would make the approximations

$$R_{xx}(t) \approx \sum_1^{IP} A_i e^{B_i t} \quad (9)$$

$$R_q(t) \approx \sum_1^{IP} A_{qi} e^{B_{qi} t} \quad (10)$$

where, in general, the A_i, B_i, A_{qi}, B_{qi} are dependent on the media properties and time angular frequency and t is a parameter describing the contour of fitting (23).

Ultimately, the complex image method allows us to write

$$G \approx \alpha\left\{\frac{e^{ikR}}{R} + \sum_{i=1}^{IP} a_i \frac{e^{ikR_i}}{R_i}\right\} \quad (11)$$

where now

$$R_i^2 = \rho^2 + (z+h+ib_i)^2. \quad (12)$$

$$a_i = A_i \exp\left(\frac{B_i T_0}{(1-iT_0)}\right) \quad (13)$$

$$b_i = \frac{B_i T_0}{k_1(1-iT_0)}. \quad (14)$$

B. Constant Q Green's Functions

For many rock and soil materials, it has been found [1] that the total effective conductivity varies with frequency in such a way as to keep the quantity

$$Q = \frac{\pi}{imag(k)\lambda} \approx \frac{\omega\epsilon}{\sigma} \quad (15)$$

approximately constant. Thus, if the complex relative permittivity is written

$$\epsilon_r = \epsilon_r' + i\epsilon_r'' = \epsilon_r'\left(1 + \frac{i}{Q}\right) \quad (16)$$

and the real permittivity is considered constant, then the complex permittivity can also be considered to be independent of frequency. In the case of water for example, the real relative permittivity is nearly constant at 80 from 0 to 3 GHz, at 20 °C. The presence of water is a significant contributor to the electromagnetic properties of many ground materials.

In the half-space case described by (3) and (5), it is possible to change the variable of integration to the angle of incidence

of the wave and eliminate the dependency on the frequency provided that the complex permittivity is not a function of frequency.

We can substitute

$$k_{1z} = k_1 \cos\ \theta_1 \tag{17}$$

$$k_{2z} = \sqrt{\epsilon_r} k_1 \cos\ \theta_2 \tag{18}$$

into (3) and (5) to obtain

$$R_{xx} = \frac{\cos\theta_1 - \sqrt{\epsilon_r}\cos\theta_2}{\cos\theta_1 + \sqrt{\epsilon_r}\cos\theta_2} \tag{19}$$

$$R_q = \frac{2\cos\theta_1}{\epsilon_r \cos\theta_1 + \sqrt{\epsilon_r}\cos\theta_2} - 1 \tag{20}$$

remembering that Snell's law gives θ_2 as a function of θ_1, hence

$$R_{12} = R_{12}(\theta_1) \neq R_{12}(\omega). \tag{21}$$

On making the change of variable in the integral

$$G = \alpha\left\{\frac{e^{ikR}}{R} + ik_1 \int_0^{\pi/2+i\infty} d\theta_1 \sin\theta_1 J_0\left(\sin\theta_1 2\pi\frac{\rho}{\lambda_1}\right) \cdot \exp\left(i\cos\theta_1 2\pi\frac{z+h}{\lambda_1}\right) R_{12}(\theta_1)\right\}. \tag{22}$$

The Green's function is now dependent on the electrical distances ρ/λ_1, $(z+h)/\lambda_1$, and the frequency dependence is reduced to the proportionality inherent in the factor k_1. Considerable computation may be saved by exploiting the frequency independence thus established when calculating the complex images.

C. Constant Q and Complex Images

Following the method of Chow *et al.*, the reflection coefficient is fitted by exponentials over a parametrically defined contour

$$C_1\colon k_{1z} = k_1\{it + (1 - t/T_0)\}, \qquad 0 < t < T_0. \tag{23}$$

Thus

$$\cos\theta_1 = it + (1 - t/T_0) \tag{24}$$

$$\sin\theta_2 = \frac{\sin\theta_1}{\sqrt{\epsilon_r}} \tag{25}$$

$$\cos\theta_2 = \sqrt{\frac{1 - (it + 1 - t/T_0)^2}{\epsilon_r}}. \tag{26}$$

It is now clear that considering the above equations for the cosines in terms of the parameter t and (19) and (20), that

$$R_q = R_q(t) \tag{27}$$

$$R_{xx} = R_{xx}(t). \tag{28}$$

The Prony method or equivalent is used to fit the exponentials to the reflection coefficient so that

$$R_{xx}(t) \approx \sum_1^{IP} A_i e^{B_i t}. \tag{29}$$

The poles and residues A_i, B_i are, thus, also independent of ω, dependence is only introduced with the parameters b_i of (14). This step can easily be deferred until the calculation of a particular frequency is required. Thus, only a single application of the Prony method is required provided that the complex permittivity is constant with frequency and the medium is not layered. In the case of layered media, standing wave terms of the form $\exp(ik_{nz}d_n)$ appear in the reflection coefficients as a result of the varying electrical thickness of the layers. Consequently, it is not possible to factor out the frequency dependent wave number k_1. The reason for our laboring of the point that the half-space model is adequate for GPR antennas and scatterers is now apparent.

III. Moment Method Model

Most of the work in this section follows the notation and methods first published by R. F. Harrington [13]. However, the integral terms in [13, eq. 99] must be denoted separately, because of the different complex images found for each of the potentials introduced by the half space. Thus, let

$$\Psi_A(m, n) = \frac{1}{\Delta x}\left\{\int_{\Delta x_n} dx' \frac{e^{ikR}}{R} + \sum_{i=1}^{IP} a_i \int_{\Delta x_n} dx' \frac{e^{ikR_i}}{R_i}\right\} \tag{30}$$

$$\Psi_\Phi(m, n^+) = \frac{1}{\Delta x}\left\{\int_{\Delta x_n} dx' \frac{e^{ikR}}{R} + \frac{1-\epsilon_r}{1+\epsilon_r}\int_{\Delta x_n} dx' \frac{e^{ikR_{qs}}}{R_{qs}} + \sum_{i=1}^{IP} aq_i \int_{\Delta_n} dx' \frac{e^{ikR_{qi}}}{R_{qi}}\right\} \tag{31}$$

where

$$R^2 = (x_m - x')^2 + a^2 \tag{32}$$

$$R_i^2 = (x_m - x')^2 + (2h + ib_i)^2 \tag{33}$$

$$R_{qs}^2 = (x_m - x')^2 + (2h)^2 \tag{34}$$

$$R_{qi}^2 = (x_m - x')^2 + (2h + ibq_i)^2 \tag{35}$$

and similar expressions apply in the case of m^+, etc.

The impedance matrix terms can then be found by substituting for the potentials in [13, eq. 99], multiplying by Δx and dividing by $I(n)$.

Thus

$$Z(m, n) = \frac{-i\omega\mu}{4\pi}\Delta x^2 \Psi_A(m, n) + \frac{1}{i\omega 4\pi\epsilon}\{\Psi_\Phi(n^-, m^+) - \Psi_\Phi(n^+, m^+) - \Psi_\Phi(n^-, m^-) + \Psi_\Phi(n^+, m^-)\}. \tag{36}$$

For the resistively loaded dipole, the diagonal impedance matrix elements are increased by the lumped impedance load at that element [14].

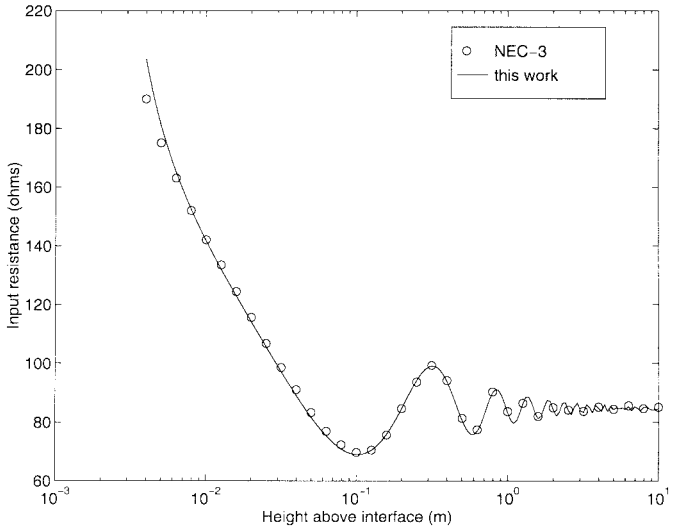

Fig. 2. Comparison with Turner: input resistance as a function of height for a horizontal half-wave dipole at 300 MHz.

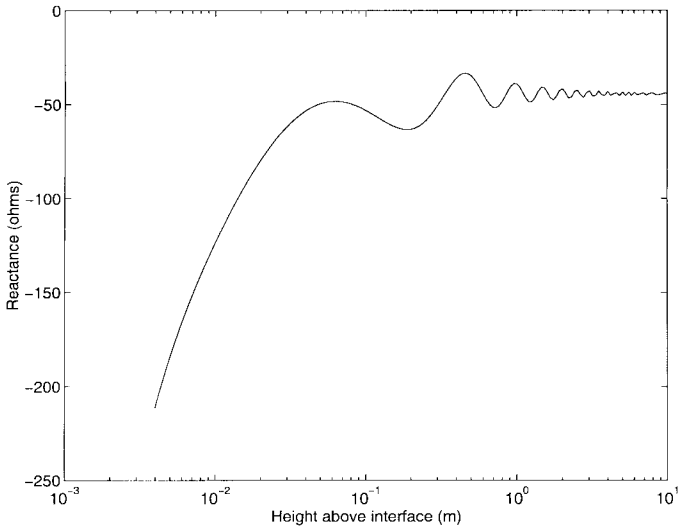

Fig. 3. Input reactance as a function of height for a horizontal half-wave dipole at 300 MHz.

IV. Results

The moment-method solution outlined in this paper was programmed using a Matlab script file. A three-term complex image fit is used for both the scalar and vector potentials, because it was observed that although a larger number of images produced more accurate Green's function for small ρ, there was a greater tendency for the function to blow up at larger values of ρ. Delta gap voltage excitation was used in preference to magnetic frill excitation because of its simplicity.

A. Comparison with NEC-3

In Turner [10], the input resistance of a 0.5-m-long dipole at 300 MHz is plotted as a function of distance from the half-space with the properties: real$(\epsilon_r) = 9.0$ and $\sigma = 0.005$ Sm^{-1}. NEC-3 was used for the calculation, assuming a radius for the dipole of 1 mm.

The data plotted by Turner was digitized and compared with the moment-method model of this work under identical conditions in Fig. 2. NEC-3 uses whole-domain basis functions and the Galerkin method rather than subsectional basis functions and point matching as used here. There is some disagreement at $h = 4$ mm. It needs to be noted that both models are in doubt in this region. The slope of the curve here is of the order of -15Ω/mm. The diameter of the wire is 2 mm. A nonsymmetrical distribution of current could easily displace the apparent height of the current filament by 0.5 mm. This would cause an error in the calculation of 7Ω. Burke *et al.* [15] also referred to the inability of a thin-wire model to correctly model behavior within a wire's radius of the interface.

The imaginary part of the input impedance was not shown in [10], but the data produced by our model is shown in Fig. 3. Ground conditions identical to those used in [11] were also used with our model for the horizontal half-wave dipole and the results agreed in both real and imaginary parts of the input impedance.

B. Pulse-Excited Resistive Dipole

In Section II-C, it was shown that if the complex permittivity of a two-layer medium is frequency independent, it is possible to reduce the computational effort in calculating responses at different frequencies by computing the image poles and residues A_i, B_i once and deferring the calculation of the complex distance parameters b_i.

This result was exploited for the resistively loaded dipole by setting the complex permittivity at $\epsilon_r = 11 + 0.1i$ and computing the current distribution of the 3.4-m dipole at 10 mm from the interface for a range of frequencies from 0 to 512 MHz. This was to enable comparison with Arcone [4], who probed current at points along a resistive dipole of length 3.4 m above a half-space of real permittivity of 11 and unstated loss. Unfortunately, the exact height of the dipole was not given, thus, the use of 10 mm in this model is arbitrary. From the resistor values given by Arcone, the resistivity parameter used was estimated to be $\Psi = 13$ in

$$\rho(x) = \frac{15\Psi}{l/2 - |x|}. \tag{37}$$

Our model used 61 pulse-basis functions and required 4 s per frequency point, running on a DEC 3000 400 Alpha work station. Arcone used a proprietary 5 ns GPR current source in his measurement. An excitation voltage source of the same form ($v(t) = \sin^2(2\pi/10^-t)$: $0 < t < 5 \times 10^{-9}$) was used in our model by transforming to the frequency domain and multiplying by the response of the antenna at a point along its length, this result was then inverse transformed to the time domain. The results of the model are shown in Fig. 4.

Some spreading of the pulses occurs, consequently the measured delay of the pulses depends on the corresponding points on the pulses chosen. If the peak is chosen, the delay of the 1.1-m point pulse is 5 ns. This indicates a pulse speed of 22 cm/ns or 0.73/ c. Alternatively, the use of the leading edge of the pulse gives a delay of 4.6 ns and an associated speed of 24 cm/ns. These speeds are slightly slower than Arcone's measured speed of 27.7 cm/ns (for which the point used on

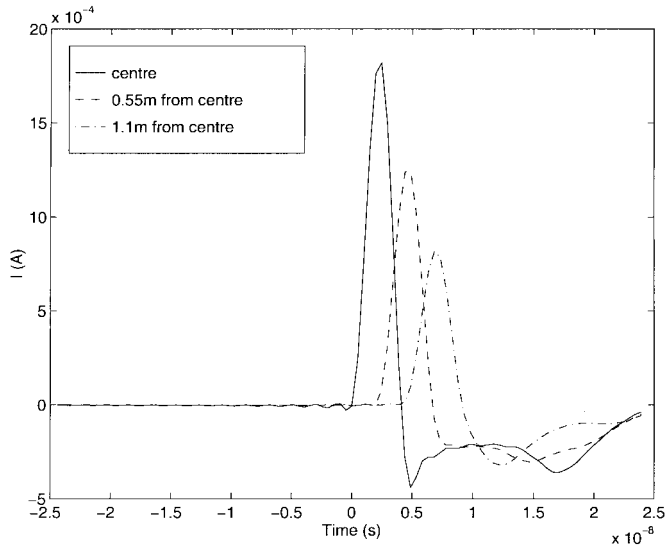

Fig. 4. Time-domain current pulses seen at equally spaced (0.55 m) points along the resistive dipole.

the pulse is not specified) possibly due to the sensitivity of the speed to distance from the interface, and the different apparent height of Arcone's dipole to that used here. The form of the pulses agree well with Fig. 4, published by Arcone of the current at the 0.5-m point.

It is interesting that although the dipole modeled is six-wavelengths long at the upper frequency, the results have adequate accuracy in spite of the inevitable failure of the complex image method for large distances close to the half-space. This probably results from the domination of near-diagonal terms in the matrix made more dominant in the half-space case where fields decay $\propto R^2$ near the interface. It appears that provided complex images are chosen that fail gracefully in the long-range case, adequate accuracy can be achieved for large structures. This indicates another advantage of the constant Q-complex image method outlined here: that a single well-behaved set of images can be selected and used over the whole frequency range.

V. Conclusions

In this paper, an efficient complex image method of moments algorithm was developed to model the current distribution on resistively loaded wire antennas close to a half-space. Using the constant Q assumption, the computation time on a work station was reduced to 4 s per frequency point with a 61 basis-function model.

In so far as the complex image method applied to wires near a half-space has been shown to give excellent agreement with other results for antennas, the work also supports the results of Vitebskiy [2] for wire scatterers and suggests the use of the constant Q method outlined here in such cases as appropriate. The method has been applied by the authors [16] to the modeling of a bowtie using triangular basis functions and the results agreed with [5], the impedance spiraling toward a quasi-static value of $152\,\Omega$ for the 60° bowtie on an $\epsilon_r = 4$ half-space.

Further work needs to be done to consider the error introduced by small absolute errors in the Green's functions at large distances and on ways to approximate the Green's functions at large distances if necessary. It may be possible to set such elements of the impedance matrix to zero with negligible loss of accuracy, resulting in a band matrix and considerable computational savings. Such an approach would implicitly recognize the transmission line behavior of wires near dense half-spaces shown by King and Smith [17].

References

[1] G. Turner and A. F. Siggins, "Constant Q attenuation of sub surface radar pulses," *Geophys.*, vol. 59, no. 8, p. 1192, Aug. 1994.
[2] S. Vitebskiy and L. Carin, "Moment-method modeling of short-pulse scattering from and the resonances of a wire buried inside a lossy dispersive half-space," *IEEE Trans. Antennas Propagat.*, vol. 43, p. 1303, Nov. 1995.
[3] S. Vitebskiy, K. Sturgess, and L. Carin, "Short-pulse scattering from buried perfectly conducting bodies of revolution," *IEEE Trans. Antennas Propagat.*, vol. 44, p. 143, Feb. 1996.
[4] S. A. Arcone, "Numerical studies of the radiation patterns of resistively loaded dipoles," *J. Appl. Geophys.*, vol. 33, p. 39, 1995.
[5] R. C. Compton, R. C. McPhedran, Z. Popovic, G. M. Rebeiz, P. P. Tong, and D. B. Rutledge, "Bow-tie antennas on a dielectric half-space: Theory and experiment," *IEEE Trans. Antennas Propagat.*, vol. AP-35, p. 622, June 1987.
[6] Y. L. Chow, J. J. Yang, D. G. Fang, and G. E. Howard, "A closed-form spatial Green's function for the thick microstrip substrate," *IEEE Trans. Microwave Theory Tech.*, vol. 39, p. 588, Mar. 1991.
[7] K. A. Michalski, "The mixed potential electric field integral equation for objects in layered media," *Archiv Elektron. Übertragungstech.* vol. 39, no. 5, p. 317, 1985.
[8] I. V. Lindell, E. Alanen, and K. Mannersalo, "Exact image method for impedance computation of antennas above the ground," *IEEE Trans. Antennas Propagat.*, vol. 33, p. 937, Sept. 1985.
[9] G. J. Burke and E. K. Miller, "Modeling antennas near to and penetrating a lossy interface," *IEEE Trans. Antennas Propagat.*, vol. 32, p. 1040, Oct. 1984.
[10] G. Turner, "The influence of subsurface properties on ground penetrating radar pulses," Ph.D. dissertation, Macquarie University, Sydney, Ausdtralia, 1993.
[11] B. D. Popovic and D. Z. Djurdjevic, "Entire-domain analysis of thin-wire antennas near or in lossy ground," *Proc. Inst. Elect. Eng. Microwaves, Antennas, Propagat.*, vol. 142, no. 3, p. 213, June 1995.
[12] W. C. Chew, *Waves and Fields in Inhomogeneous Media.* New York: IEEE Press, 1995.
[13] R. F. Harrying, *Field Computation by Moment Methods.* New York: Macmillan, 1968.
[14] R. Mittra, Ed., *Computer Techniques for Electromagnetics.* Washington, DC: Hemisphere, 1987.
[15] G. J. Burke, W. A. Johnson, and E. K. Miller, "Modeling of simple antennas near to and penetrating an interface," *Proc. IEEE*, vol. 71, p. 174, Jan. 1983.
[16] C. J. Leat, N. V. Shuley, and G. F. Stickley, "Complex images + constant Q = a fast GPR antenna model," in *Proc. 7th Int. Conf. Ground Penetrating Radar*, Lawrence, KS, May 1998, pp. 75–80.
[17] R. W. P. King and G. S. Smith, *Antennas in Matter*. Cambridge, MA: MIT Press, 1981.

Christopher J. Leat was born in Cairns, Australia, in 1963. He received the B.S. degree (first-class honors) in physics in 1994 from the University of Queensland, Australia. He is currently working toward the Ph.D. degree in the Department of Electrical and Computer Engineering, University of Queensland

Prior to commencing study, he worked as an Electronics Technician at the NASA DSCC at Tidbinbilla, Australia. Since 1995 he worked as an Associate of the Cooperative Research Centre for Sensor Signal and Information Processing, where his responsibilities have been to develop electromagnetic (EM) models for and understanding of antenna behavior for GPR systems. His interests include the propagation of EM waves from sources near half-spaces and the design principles of broad-band radiating structures.

Nicholas V. Shuley, for a photograph and biography, see p. 1280 of the September 1993 issue of this TRANSACTIONS.

Glen F. Stickley received the B.Sc. (first-class honors) and Ph.D. degrees in applied physics from the University of Queensland, Australia, in 1987 and 1996, respectively.

He joined the Cooperative Research Centre for Sensor Signal and Information Processing (CSSIP) in 1993, where he works on stepped frequency ground penetrating radar and radar interferometry for highwall monitoring.